Insight into non-covalent interactions in a tetrachlorocadmate salt with promising NLO properties: Experimental and computational analysis

Ikram Jomaa, Noureddine Issaoui, Thierry Roisnel, Houda Marouani

Insight into non-covalent interactions in a tetrachlorocadmate salt with promising NLO properties: Experimental and computational analysis

Ikram Jomaa[a], Noureddine Issaoui[b], Thierry Roisnel[c] and Houda Marouani[a]

[a]Université de Carthage, Faculté des Sciences de Bizerte, LR13ES08 Laboratoire de Chimie des Matériaux, 7021, Bizerte, Tunisie

[b]University of Monastir, Laboratory of Quantum and Statistical Physics LR18ES18, Faculty of Sciences, Monastir 5079, Tunisia

[c]Univ Rennes, CNRS, ISCR (Institut des Sciences Chimiques de Rennes) – UMR 6226, F-35000 Rennes, France

*Correspondence e-mail: houdamarouani2015@gmail.com

Abstract

This paper deals with the crystal structure of the new non-centrosymmetric organic-inorganic hybrid material, $(C_6H_{14}N)_2[CdCl_4]$. Single crystal X-ray diffraction analysis shows that this compound crystallizes in the orthorhombic system, with the space group $Cmc2_1$ and the following parameters a = 27.257 (2) Å, b = 8.3560 (6) Å, c = 7.8872 (5) Å, V = 1796.4 (2) $Å^3$ and Z = 4. The structure provides a new interesting example of infinite inorganic chains of $[CdCl_5]_n$ following the $\vec{c}$ crystallographic direction. The monoprotonated cyclohexylammonium cations are linked to the anions via electrostatic, multiple bifurcated N—H…Cl hydrogen bonds and van der Waals interactions. To support experimental results, DFT calculations have been accomplished via the B3LYP method with 6-311++G(d,p) and LANL2DZ basis set on molecular geometry, vibrational and electronic properties. The non-covalent interactions were studied through AIM and RDG analysis and quantitatively using the Hirshfeld surfaces (HS) associated with 2D fingerprint plots. The NLO properties have been also investigated by DFT and compared to the urea reference

Keywords: Cd(II) complex: X-ray diffraction; DFT calculations; Hirshfeld surface; AIM; NLO.

1. Introduction

Organo-metal halides assembly investigation represents for a quite while one of the most active areas of chemical research and material science due to their designable and tuneable characteristics as well as their potential applications in numerous fields including catalysis **[1]**, biochemistry **[2]**, magnetism, electrical conductivity **[3]**, and nonlinear optical (NLO) devices **[4]**.

In particular, Halogenocadmates(II) crystal chemistry is exceptionally diverse due to the fact that Cd^{2+} is a d^{10} metal ion. It demonstrated a propensity for forming a variety of crystalline structures by self-assembling from suitable solution mixtures, their structural flexibility enables a great variety of structural archetypes to be constructed in the form of one-dimensional linear chains **[5],** two-dimensional layers **[6],** and ribbon-like structures **[7].**
Else, cyclohexylammonium organic entities have been found to be a useful reagent for metal ions, due to their reactivity and adaptability in stabilizing various structures **[8,9].** Cyclohexylammonium organic molecules can be associated with chlorocadmates to produce systems with a potentially forceful network of hydrogen bond interactions.

From a structural point of view, two categories of organo-metal halides hybrids are distinguished **[10]**: Class I where both organic and inorganic constituents are linked by weak non covalent interactions while the components of class II hybrids are combined through stronger covalent bonds. The weakness of the bonds in Class I is responsible for the flexibility and dynamics of structures. Moreover, the assembly of organo-metal halides can create noncentrosymmetric materials with important nonlinear optical coefficients and specific physical and chemical properties. Developments in the field of non-linear optics play a major role in the field of photonics including optical information processing, sensor protector applications, data storage, etc **[4]**.

In the present contribution to the above materials, generally expressed as $(R–NH_3)_2MX_4$ (where R = is an organic cation, M = divalent metal, and X = halogen), and that consists of an extended network of metal halide tetrahedra or octahedra (typically being observed), sharing faces, edges, or vertex and alternating with a monolayer or multilayer organic group, we report the crystal structure study in detail of $(C_6H_{14}N)_2[CdCl_4]$ compound, Hirshfeld surface analysis, and fingerprints plots calculations.

Furthermore, even though computational analysis has become an impressive characterization approach only a modest number of papers report some theoretical

calculations of organic-chlorocadmates compounds **[11,12]**. So here a state-of-the-art computational study was undertaken on the occurrence and nature of weak non covalent interactions in the assembly of the title structure, and have been as well combined with experimental results throughout this work for structural, vibratory, and electronic characterization. Topological properties and RDG analysis were also computed.

2. Experimental details

2.1. Synthesis and crystallization

Metal/amine molar ratio 1:2 solution of: $CdCl_2.H_2O$ (0.201 g, 1 mmol, Aldrich, purity 98%) mixed in dilute HCl (5 mL, 3 M) was added drop wise to a solution of cyclohexylamine (0.198 g, 2 mmol, Aldrich, purity 99%) dissolved in ethanol. The mixture is left under stirring at room temperature for 30 minutes. One week later well-defined single crystals of $(C_6H_{14}N)_2[CdCl_4]$ were formed. Schematically the reaction can be written as follow:

$$2\ (C_6H_{13}N) + \ CdCl_2.H_2O + 2\ HCl \xrightarrow{EtOH\ /\ H_2O} (C_6H_{14}N)_2CdCl_4 \ + \ H_2O$$

Elemental analysis, calc. (found): C, 31.68% (31.52); H, 6.16% (6.12); N, 6.16% (6.10); Cd, 24.73% (24.79).

2.2. X-ray data collection and physical measurements

Data were collected at 150 K using an APEXII Bruker-AXS diffractometer equipped with Graphite monochromator and MoKα radiation (λ = 0.71073 Å). Absorption corrections were performed using the multi-scan technique using the SADABS program **[13].** The total number of measured reflections was 7344 among which 2013, were independent and 1985 had the intensity I >2σ(I). The structure was solved with SHELXT **[14],** which revealed the position of all non-hydrogen atoms, and then refined with full-matrix least-square methods based on F^2 (SHELXL) **[15]** included in the WINGX program **[16].** A final refinement on F^2 converged at $R(F^2)$ = 0.044 and $wR(F^2)$ = 0.114. A summary of the crystal data and the structure refinement parameters are included in **Table 1**. An ORTEP drawing of the asymmetric unit is exposed in **Fig. 1a**.

IR spectrum was registered at room temperature in the frequency range 4000-400 cm^{-1} with a Perkin-Elmer FT-IR 1000 spectrometerequipped with a diamond micro-ATR access.

2.3. Computational details

Initially, thex-ray structure of $(C_6H_{14}N)_2[CdCl_4]$ compound imported on a CIF format was optimized in the gas phase with the Gaussian 09 software package **[17].**

All the quantum-chemical calculations have been performed via the hybrid B3LYP (Becke-three-parameter hybrid exchange functional combined with the Lee-Yang-Parr correlation functional) **[18, 19]** levels, the 6-311++G(d,p) basis set was used for all atoms except for the cadmium atom, the LANL2DZ basis set and effective core potentials (ECPs) (LANL2DZ basis and ECP built-in) have been used to represent the metal. Vibrational frequencies were calculated at the same level to ensure that each stationary point was a true minimum. We choose this functional because experimental and theoretical values are in good agreement. We have used the same method in similar compounds and have found good results **[11, 20]**.

On the other hand, the hybrid exchange-correlation functional named CAM-B3LYP combines the hybrid qualities of B3LYP and the long-range correction. Many theoretical studies show that CAM-B3LYP yields atomization energies of similar quality to those from B3LYP, while also performing well for charge transfer excitations in some models like in the case of organic compounds, which B3LYP underestimates enormously. In our case, in this paper, we study a hybrid compound which is formed by an organic and inorganic entity. For this type of these compounds, in our previous works **[21,22]**, we have tried many methods, studied the dispersion effect and we have found that this functional haven't any effect in the energies or have very negligible effect.

Hirshfeld surfaces mapped with d_{norm} and their associated 2D fingerprint were plotted using Crystal Explorer version 3.1 software **[23]**. The topological analysis was carried out with the Multiwfn program **[24]** while the reduced density gradient of the title compound is graphed by Multiwfn and plotted by the VMD program **[25].** The optimized molecular structure is used to perform HOMO- LUMO distributions and MEP analysis.

3. Results and discussion

3.1. X-ray diffraction and geometry optimization

Single crystal X-ray diffraction analysis reveals that the asymmetric unit of the title material is formed by a monoprotonated cationic entity which is the cyclohexylammonium ($C_6H_{11}NH_3^+$) and an anionic entity which is $[CdCl_3]^-$, where Cd, Cl2 and Cl3 are in special positions in the mirror x = 0 and x = 1/2. By symmetry, the pyramid with a square base is

formed. Otherwise, the organic entity exhibits a disorder manifested by the thermal agitation of all hydrogen, nitrogen, and carbon atoms.

The optimized molecular structure of $(C_6H_{14}N)_2CdCl_4$ compound is given in **Fig. 1b**. A comparison between selected optimized geometrical parameters, with experimental X-ray crystallographic parameters, is given in **Table 2**.

Interatomic bond lengths and angles of the organic group are in full agreement with those found in other compounds containing the same organic cation **[8,9]**. The protonation on the N site of the cation is confirmed from the elongated C-N bond distance (d_{N-C} = 1.564 (19)Å). The variation of the optimized C-C bond length is from 1.528 Å to1.549 Å and by XRD from 1.18 (3) to 1.60 (3) Å. Cyclohexylammonium adopts a chair conformation with an ammonium group in the equatorial position, the bond angles (C-C-C) were calculated between 110.3-108.1° and (N-C-C) observed by XRD between 97.4 ° and 101.3 ° and calculated at 105.4 °. Assessment of the inorganic geometrical features shows that the Cd(II) ion exhibits a slightlydistorted square pyramid configuration with experimental and calculated Cd-Cl bond lengths ranging from 2.489 (3)-2.892 (3) Å and between 2.435-2.898 Å, respectively. The coordination geometry around Cd(II) ion shows the typical axial compression of the square pyramid geometry, with the Cd-Cl distance equal to 2.489 (3) Å. The Cl-Cd-Cl bond angles are calculated between 85.83 and 153.22°, and observed by XRD between 83.30 (6) to 156.53 (9)°. These values are comparable with those reported in related halogenocadmates **[7,12].** The slight discrepancies observed between the computed and the experimental bond lengths and angles can be explained by the fact that the calculations relate to an isolated molecule, whereas the experimental results correspond to interacting molecules in the crystal lattice.

Further, we can propose a simple angular parameter used for penta-coordinate materials and defined by Alvarez **[26]** as:

$$\tau = \frac{\alpha - \beta}{60}$$

Where α and β are the two largest Cl–Cd–Cl bond angles, with [β<α].Thus, any structure intermediate between trigonal bipyramid and square pyramid must have an angular parameter in the range$0 \leq \tau \leq 1$, a perfect trigonal bipyramid presents (α = 180 and β = 120) resulting in τ= 1 while an ideal square pyramid has α = β and its angular parameter is τ = 0.

Here:

$$\tau = \frac{156.53 - 142.89}{60} = 0.227$$

So we can admit that the square pyramid $CdCl_5$ is slightly distorted.

The inorganic network consists of 1-D polymeric chains of square-pyramidal $CdCl_5$ vertex-sharing units developing parallel to the $(\vec{b},\vec{c})$ plane. The cationic layers are regularly intercalated between these anionic chains, the cohesion of the cations with the $[CdCl_5]_n$ chains is ensured through N–H…Cl hydrogen bonds resulting in the stabilization of the hybrid structure (**Fig. 2a**). A perspective view of the inorganic part (**Fig. 2b**), shows that the one-dimensional polymeric chains of square-pyramidal $CdCl_5$ units are located around x = 0 and 1/2. These entities are linked to each other via Cl2 and $Cl2^{ii}$ chlorine atoms (ii: *x*, −*y*+1, *z*−1/2) by vertex-sharing to form zigzag chains (**Fig. 2c**). Similar vertex-sharing example was also observed in $(C_5N_2H_9)CdCl_3$**[5].**

Two neighboring chains are further connected into a 2D supramolecular network by means of N-H… Cl type bonds with donor-acceptor distances ranging from 3.199 (5) to 3.372 (6) Å (Details in **Table 3**), three of which are bifurcated: N1A—H1A1…($Cl2^{ii}$, $Cl3^{i}$), N1B—H1B2…($Cl1^{iii}$, $Cl3^{iii}$) (iii: *x*, −*y*+1, *z*+1/2) and N1B—H1B3…(Cl1, $Cl2^{ii}$) (ii: *x*, −*y*+1, *z*−1/2), forming $R_6^2(8)$, $R_1^5(6)$, $R_1^5(6)$, $R_3^3(6)$, $R_6^4(10)$, $R_2^2(4)$, $R_6^6(12)$ and $R_{12}^7(19)$ motifs (**Figs. 2d&e**).

3.2. Hirshfeld surface analysis

Here, the Hirshfeld surface (HS) and their associated 2D fingerprint plots analysis of the asymmetric unit was undertaken as a systematic computational investigation method, that provides insight, quantification and exploration of intermolecular close contacts present within the crystal packing.The HS mapped over d_{norm} of $(C_6H_{14}N)_2CdCl_4$ illustrated in **Fig. 3**, allows a surface with a color scheme to be displayed, where dark red spots highlight the shortest intermolecular contacts that are attributed to N-H…Cl interactions, the white areas mark the contacts around the van der Waals separation and the blue areas illustrate the longest intermolecular contacts in the structure.

Further, the intermolecular interactions involved within the structures are also visible in the full 2D fingerprint (**Fig. 4a**) that can be decomposed (**Fig.4b,c,d,e,f**) to quantify individual contributions and highlight pairs of atoms in close contact.

In fact, As expected, the major contribution (55.1%) comes from H…Cl/Cl…H intercontacts that appear as two pointed symmetrical spikes with a maximum sum of $d_e + d_i$ ~ 2.2 Å less than the sum of the VdW radii of the chlorine atom and the hydrogen atom (1.75 + 1.09 = 2.84 Å). H… H contacts comprise 39.7% of the entire HS. They are characterized by

a single broad peak in the middle of the scattered points, which point towards the origin and correspond to ($d_e + d_i \sim 1.3$ Å), a value less than the sum of the VdW radii of the atoms of hydrogen (1.09 + 1.09 = 2.18 Å). The Cd… Cl / Cl… Cd contacts which occupy 3.7% of the entire HS show on its 2D graph the presence of a pair of symmetrical wings ($d_e = d_i \sim 1.4$ Å) value less than the sum of the VdW radii of the atoms involved (Cd: 1.58 Å Cl: 1.75 Å).

These findings affirm that the last three intercontact are considered to be close contacts.

The H… Cd / Cd… H contacts represent 1.1% of the total HS and which correspond to $d_e + d_i \sim 3.6$ Å> (2.67 Å = 1.09 + 1.58). These contacts are considered non-close contact. Fig.5 f, shows the pairs (d_i, d_e) of chlorine atoms. It can be seen that ($d_e + d_i \sim 3.6$ Å) > 3.5 Å, the sum of the VdW radii of the chlorine atoms. This reveals the absence of close Cl ... Cl contacts.

Subsequently, the enrichment ratio was calculated to point up the contacts statistically favored (ER close to unity) in the crystal packing. The calculated values of ER are given in **Table S1**. The value ($ER_{HCl} = 1.36$) greater than unity, of H… Cl / Cl… H contacts show the propensity to form N-H ... Cl hydrogen bonds. H ... H contacts appear with an enrichment ratio close to unity (0.86), this value agrees well with Jelch's expectation **[27].** These contacts occupy more than half of HS with $S_H = 67.8\%$. On the other hand, the Cd ... Cl / Cl ... Cd contacts are extremely enriched (ER = 2.59), they represent a major attraction in the crystal despite their small surface area. The Cl… Cl, and H… Cd / Cd… H contacts represent as well a low contribution on the HS (0.4% and 1.1%). Despite the lowness of these percentages, we can suggest animprovement of the crystalline stability owing to their cumulative effect.

Such visual analysis of intermolecular interactions is consistent with those found by X-ray diffraction analysis.

3.3. Vibrational analysis

The vibrational properties of the $(C_6H_{14}N)_2[CdCl_4]$hybrid material were discussed based on a vibrational study using experimental and calculated infrared spectroscopy. The experimental IR spectrum measured between 400 and 4000 cm^{-1} at room temperature and simulated using B3LYP/LanL2DZ basis set are shown in **Fig. 5**. For vibrational frequency, uniform scaling factors were adopted: frequencies below 1700 are multiplied by 0.983, so that greater than 1700 are multiplied by 0.958 **[11,28-31]**. This correction is made to find a good

agreement with the experimental frequencies. The correlation between observed and theoretical spectra is reasonable; the differences observed especially in the region of higher wavenumbers can be easily attributed to the calculations because these were performed in the gas phase where the crystalline packing forces were not considered. The detailed assignment of the characteristic bands is essentially based on comparisons with data previously reported for similar materials. Brief discussions of the assignments for the most important functional groups are presented below.

3.3.1. $[CdCl_4^{2-}]$ vibrations

According to the theoretical calculations and by reference to other compounds including the chlorocadmate anion **[11,12]**, it is found that the inorganic entity leads to vibrations below 500 cm^{-1}. The asymmetric and symmetric stretching of Cd-Cl appeared at 189 and 174 cm^{-1}, respectively. The band corresponding to the bending mode of Cl-Cd-Cl appeared in the 74 cm^{-1}.

3.3.2. $C_6H_{11}NH_3^+$ vibrations

The N-H asymmetric and symmetric stretching vibrations are observed in the high-frequency region between 3444 and 3119 cm^{-1}. The DFT computations give the frequency of these bands between 3495 and 3104 cm^{-1}.The bands observed at 1598 and 1565 cm^{-1} are respectively assigned to the asymmetric and symmetric bending modeof N-H.The corresponding bands are calculated to be found at 1605 and 1563 cm^{-1}. The bandsof medium intensities between 1486-1454 cm^{-1} are attributed to the characteristic NH_3^+ asymmetric and symmetric stretching vibrations and predicted at 1503 and 1422 cm^{-1}. In cyclohexylammonium perchlorate **[21]** these modes are observed nearly in the same region.

The asymmetric and symmetric stretching vibrations of ($-CH_2$) are observed at 2936 and 2858 cm^{-1} respectively. Whereas, these vibrations are calculated at ν_{as} = 2921 cm^{-1} and ν_s = 2880 cm^{-1}. The bands that lie between1121 and 1007 cm^{-1} in the experimental spectrum correspond to the C-N stretching. The same vibration is calculated between 1145and 1003 cm^{-1} by DFT level. Withal, the bands that appear around 547 and 455 cm^{-1} are attributed to the out of plane vibration modes of the δ(C-C) et δ(C-N) groups and predicted to be found in region 565-476 cm^{-1}.

3.4. Quantum theory of AIMs and RDG analysis

R. Bader **[32]** suggests that the presence of BCPs and the bonding paths between two atoms confirm the interaction between them. The graphical representation of the AIM analysis of the $(C_6H_{14}N)_2CdCl_4$ is illustrated in **Fig.6**, here the BCPs are located along the Cl… H bonds.

AIM analysis reveals that the title material is stabilized by eight hydrogen bonds that meet Koch and Popelier criteria **[32,33]** and that the interactions Cl47… H9, Cl47… H2, Cl44… H21, Cl44… H4 exhibit topological properties similar to the interactions Cl47… H30, Cl47… H23, Cl46… H42, Cl46… H25. The corresponding geometric, energetic, and topological parameters of the BCPs are collated in **Table S2**. With reference to Rozas criteria **[34],** all of the eight hydrogen bonds are considered weak since the Laplacian and the energy density values are positive. Positive Laplacian values that vary from 0.05617 to 0.00874 a.u. indicate as well the depletion of electronic charge along the binding path. The observed density for the Cl44… H4 or Cl46… H25 interactions (0.019515-0.019514 a.u.) is the highest probably because the distance between these two atoms is the smallest. Thus these last two interactions are considered to be the strongest according to the value of the calculated hydrogen bond energy which is of the order of -13.91126 $kJ.mol^{-1}$.

Further, the non-covalent interactions (NCIs) of a stabilizing or destabilizing nature existing in the $(C_6H_{14}N)_2CdCl_4$ compound were also characterized by the NCI plot computational tool (RDG) that permits to assess the self-assembled structure. The non-covalent interactions are represented by isosurfaces instead of critical points.The illustration of various interactions types in the $(C_6H_{14}N)_2CdCl_4$ structure is presented in **Figs. 7a** and **b.**

According to **Fig. 7a,** the attractive, van der Waals and repulsive interactions appear as blue, green, and red scattered spikes, respectively. Each individual peak corresponds to a single non-covalent interaction. The RDG peaks towards -0.02, -0.025 and -0.045 u.a with sign $(\lambda 2)\rho$ correspond to a strong attractive interaction confirmed also by the low-density values.

Regarding the isosurface color scheme in **Fig. 7b**, light blue spots are observed between the hydrogen and chlorine atoms, which justify the strong attractive interaction NH ... Cl. The differences in hydrogen bond strength can be seen from the depth of the blue, the absence of the strong blue colored isosurface clearly indicates that the structure of $(C_6H_{14}N)_2CdCl_4$ does not exhibit strong hydrogen bonds.Interactions that appear as green patches around the anion are attributed to van der Waals interactions. The elliptical red plaque

located at the center of the cycle is linked to repulsive interactions that show a strong steric effect. These results are consistent with those of the AIM analysis.

3.5. Molecular electrostatic potential (MEP)

The electrostaticpotential surface is relevant to electrondensitytherebyitisusedto predictthe reaction sites or attackswithpotentialelectrophiles or nucleophiles as well as hydrogen bonding interactions. The electrostatic potential at any point $\vec{r}$ in the space surrounding a molecule can be expressed as **[35]:**

$$V(r)= \sum_A \frac{Z_A}{|R_A - r|} - \int \frac{\boldsymbol{\rho}(\boldsymbol{r}')\mathrm{d}r'}{|r' - r|}$$

Where Z_A is the charge of the nucleus A located at $\vec{R}_A$ and $\rho(\overrightarrow{r'})$ is the molecular electron density function. The sign of $V(\vec{r})$ at a particular region depends upon whether the effect of the nucleus or the electronsis dominant there :

- If $V(\vec{r}) > 0$: region of strong attraction, electrophilic sites (blue color).
- If $V(\vec{r}) < 0$: region of strong repulsion, nucleophilic sites (red color).
- Neutral and slightlyneutralpotential (green and yellowcolorrespectively).

The electronic distribution can be easily seen from the different colorations of their mapped surfaces, **Fig.8** illustrates the mapped MEP surfaces of $(C_6H_{14}N)_2[CdCl_4]$compound. The area of negative potentials (excess in electrons) defined by a red color is associated with $[CdCl_4]^{2-}$ group as a nucleophilic site while the most positive potential (deficient in electrons) defined by a blue color is observed at the level of the hydrogen atoms, as expected due to its higher donor capacity, especially near the $-NH_3^+$ group of the cyclohexylammonium cation so candidate for nucleophilic attacks.

On the cations side chain a notable yellow color typical of slightly inert region is observed. This confirms the existence of intermolecular N-H···Cl interactions between the two organic cations and the inorganic anion in the compound understudy. The electrophilic and nucleophilic sites explain the formation of Hydrogen bonds, which is defined as being a donor-acceptor interaction. It demonstrates that the electrostatic potential of the donor becomes less negative as the acceptor becomes more negative **[36].**

3.6. Frontier orbitals and chemical quantum descriptors

The 3D plots of HOMO-1, HOMO, LUMO, and LUMO+1 of $(C_6H_{14}N)_2[CdCl_4]$ are provided in **Fig. 9**, the red and the green colors of the plots correspondto the positive and the negative phase, respectively. Orbital analysis revealed that the HOMO components are

located on the anionic part, while the LUMO components are mainly located on the NH_3^+ group of the organic cation and on the [$CdCl_4$] group. The energy level of the HOMO orbital is equal to-5.14eV and the energy level of the LUMO orbital is equal to -1.51eV, which gives an energy gap of about 3.63 eV. This value agrees very well with the corresponding energy gap reported earlier of other organic chlorocadmate(II) compounds **[11]**.

Through the results of the calculated HOMO and LUMO energies and by means of equations reported in the literature **[6,8]**, the global chemical reactivity descriptors (The electronegativity (χ), hardness (η), softness (S), electrophilicity index (ψ) and the chemical potential (μ)) can be defined. The results of this surveyusing the TD-DFT method are gathered in **Table 4**.

The energies of HOMO and LUMO orbitals of the studied compound are related to the ionization potential I and to the electronic affinity A, respectivelyby the following relationships: $I = -E_{HOMO}$ and $A = -E_{LUMO}$. All the determined energies in the gas phase of $(C_6H_{14}N)_2[CdCl_4]$ material were found to be negative as well as the chemical potential. Hardness and chemical softness are also good indicators of chemical stability; here the material has hardness equal to 1.81eV and chemical softness equal to 0.27 eV. The electrophile index ψ = 3.05 eV is relatively high, so we can conclude that these findings are an index of high kinetic stability and low chemical reactivity of the crystal structure.

3.7. Non-linear optical properties

The need for the investigation of hybrids was to promote new sophisticated materials with targeted physical and chemical features **[11]**, in the NLO application field, organic-inorganic complex crystals have been developed to combine the advantages of inorganic crystals, such as good stability and resistance to physical andchemical attack, with the advantages of organic crystals, in order to retain the high NLO efficiency of organic materials and overcome its shortcoming.

The electric dipole moment, polarizability, and first-order hyperpolarizability values of the title materialusing DFT/B3LYP/LANL2DZ method are grouped in **Table 5**. (α) and (β) values of the Gaussian output are in atomic units (a.u.), so they have been converted into electronic units (esu) (α; 1 a.u. = 0.1482×10^{-24} esu, β; 1 a.u. = 8.6393×10^{-33} esu).

The quantities cited (**Table 5**) are obtained from the following equations:

$$\mu = (\mu_x^2 + \mu_y^2 + \mu_z^2)^{1/2}$$

$$\alpha_{tot} = \frac{1}{3}(\alpha_{xx} + \alpha_{yy} + \alpha_{zz})$$

$$\beta = [(\beta_{xxx} + \beta_{xyy} + \beta_{xzz})^2 + (\beta_{yyy} + \beta_{yzz} + \beta_{yxx})^2 + (\beta_{zzz} + \beta_{zxx} + \beta_{zyy})^2]^{1/2}$$

The calculated values of the dipole moment, the polarizability and the first-order hyperpolarizability of $(C_6H_{14}N)_2CdCl_4$ compound are respectively 10.15 Debye, 35.75×10^{-24} esu, and 2776.41×10^{-33} esu. The comparison of these values with the urea which is a standard NLO reference material (μ= 1.3732 Debye, α= 5.0477×10^{-24}esu, β= 372.8×10^{-33}esu) shows a large value of β_{tot} which is a bit higher than7x β_{urea} indicating important second-order optical effects. According to the literature **[12]**, hydrogen bonds play an important role not only in the generation of the crystal structure and its stability, but also they contribute to the improvement of the hyperpolarizability of molecular systems and therefore the enhancement of the optical properties of the material.

The dipole moment is 7 times higher than μ_{urea} which can be explained by the non-centrosymmetric nature of this molecule. The highest absolute value of the dipole moment is observed for the component μ_z in this direction the value is equal to 8.61 D, while the polarizability is mainly along the x-axis (α_{xx}= 286.790 a.u.). The calculated polarizability α_{tot} is found to be higher than $7\alpha_{urea}$. All these results nominate the $(C_6H_{14}N)_2CdCl_4$ as a good material for NLO application.

4. Conclusion

This contribution is intended to cast light on the non-covalent weak interactions and on the NLO properties of the $(C_6H_{14}N)_2CdCl_4$ material. Structural analysis has shown that noncovalent assembly is mainly controlled by N—H…Cl H-bonds. The entire supramolecular self-assembly and consequent cooperatively of weak noncovalent interactions have been analyzed in detail (AIM, RDG, and MEP analysis) and further quantified by theoretical Hirshfeld surface analysis. The theoretical investigations support the experimental findings. The HOMO and LUMO energies and other calculated quantum parameters reveal the hardness and the great stability of the material. The assignment of the vibrational bands wasprecisely performed by comparison with the vibration modes frequencies of homologous compounds and with the theoretical results. The compound is a good nonlinear optical material candidate.

Acknowledgements

We are grateful to the Tunisian Ministry of Higher Education Scientific Research for the provided support.

Supplementary Information: Tables S1-S2. Crystallographic data for the structural analysis have been deposited at the Cambridge Crystallographic Data Centre, CCDC No 2068977. These data can be obtained free of charge via https: //www.ccdc.cam.ac.uk/conts /retri eving.html, or from the CCDC, 12 Union Road, Cambridge, CB2 1EZ, UK: fax: (+44) 01223-336-033; e-mail: deposit@ccdc.cam.ac.

References

[1] Y. Li, Y. Yu, L. Wu, J. Zhi, Processable polyaniline/titania nanocomposites with good photocatalytic and conductivity properties prepared via peroxotitanium complex catalyzed emulsion polymerization approach, Appl. Surf. Sci. 273 (2013) 135-143.

[2] L.M. Novena, S.S. Kumar, S. Athimoolam, Improved solubility and bioactivity of theophylline (a bronchodilator drug) through its new nitrate salt analyzed by experimental and theoretical approaches, J. Mol. Struct. 1116 (2016) 45-55.

[3] P. Englebienne, A.V. Hoonacker, Gold-conductive polymer nanoparticles: a hybrid material with enhanced photonic reactivity to environmental stimuli, J. Colloid Interface Sci. 292 (2) (2005) 445-454.

[4] S. Suresh, A. Ramanand, D. Jayaraman, P. Mani, Review on theoretical aspect of nonlinear optics, Rev. Adv. Mater. Sci. 30 (2012) 175-183.

[5] K. Chu, Y. H. Zhou, J. L. Song, C. Zhang, An ABX3 organic–inorganic perovskite-type material with the formula $(C_5N_2H_9)CdCl_3$: Application for detection of volatile organic solvent molecules, Polyhedron 131 (2017) 22-26.

[6] Y. Jin, C. H. Yu, W. Zhang, Structural diversity of a series of chlorocadmate(II) and chlorocuprate(II) complexes based on benzylamine and its N-methylatedderivatives, J. Coord. Chem., 67(2014) 1156.

[7] M. Hajji, J. S. Al-Otaibi, M. Belkhiria, S. Dhifaoui, M. A. Habib, S. M. H Elmgirhi, H. Mtiraoui, R. Bel-Hadj-Tahar, M. Msaddek, T. Guerfel, Structural and computational analyses

of a 2-propanolammonium-chlorocadmate(II) assembly: Pivotal role of hydrogen bonding and H—H interactions, J. Mol. Struct. 1223 (2021) 128998.

[8] S.S. Yun, H.S. Moon, C.H. Kim, S.G. Lee, Synthesis and crystal structure of bis(dicyclohexylammonium) Tetracyanonickel(II), J. Coord. Chem.,57 (2004).

[9] M. Sarr, C. Merkens, A. Diassé-Sarr, L. Diop, U. Englert, Bis(cyclohexylammonium) tetra-chlorido-diphenyl-stannate(IV), Acta Cryst., E70 (2014) m220-m221.

[10] K. Rurack , R. Martínez-Máñez , The Supramolecular Chemistry of Organic-Inorganic Hybrid Materials, John Wiley & Sons, Inc., Hoboken, NJ, USA, 2010.

[11] I. Jomaa , O. Noureddine , S. Gatfaoui , N. Issaoui , T. Roisnel , H. Marouani , Experimental, computational, and in silico analysis of $(C_8H_{14}N_2)_2[CdCl_6]$ compound, J. Mol. Struct. 1213 (2020) 128186.

[12] L.M. Yang, Y. Liu, L.M. Man, J.R. Zhou, X.P. Liu, C.L. Ni, Crystal structure,vibrational spectra, optical properties and density functional theoretical approach of $[Bz\text{-}4\text{-}NH_2Py]_4[CdCl_4]_2.H_2O$, Vib. Spectrosc. 93 (2017) 23-28.

[13] Bruker, APEX2, SAINT and SADABS, Bruker AXS Inc., Madison, Wisconsin, USA, 2006.

[14] G. M. Sheldrick, SHELXT-Integrated space-group and crystal-structure determination, Acta Cryst. A71 (2015) 3-8.

[15] G.M. Sheldrick, Crystal structure refinement with SHELXL, Acta Crystallogr. C71 (2015) 3-8.

[16] L.J. Farrugia, WinGX and ORTEP for windows: an update, J. Appl. Cryst. 45 (2012) 849-854.

[17] M.J. Frisch, G.W. Trucks, H.B. Schlegel, G.E. Scuseria, M.A. Robb, J.R. Cheeseman, G. Scalmani, V. Barone, B. Mennucci, G.A. Petersson, H. Nakatsuji, M. Caricato, X. Li, H.P. Hratchian, A.F. Izmaylov, J. Bloino, G. Zheng, J.L. Sonnenberg, M. Hada, M. Ehara, K. Toyota, R. Fukuda, J. Hasegawa, M. Ishida, T. Nakajima, Y. Honda, O. Kitao, H. Nakai, T. Vreven, J.A. Montgomery Jr., J.E. Peralta, F. Ogliaro, M. Bearpark, J.J. Heyd, E. Brothers, K.N. Kudin, V.N. Staroverov, R. Kobayashi, J. Normand, K. Raghavachari, A. Rendell, J.C. Burant, S.S. Iyengar, J. Tomasi, M. Cossi, N. Rega, J.M. Millam, M. Klene, J.E. Knox, J.B.

Cross, V. Bakken, C. Adamo, J. Jaramillo, R. Gomperts, R.E. Stratmann, O. Yazyev, A.J. Austin, R. Cammi, C. Pomelli, J.W. Ochterski, R.L. Martin, K. Morokuma, V.G. Zakrzewski, G.A. Voth, P. Salvador, J.J. Dannenberg, S. Dapprich, A.D. Daniels, O. Farkas, J.B. Foresman, J.V. Ortiz, J. Cioslowski, D.J. Fox, Gaussian, Inc., Wallingford CT, 2009.

[18] A.D. Becke, Becke's three parameter hybrid method using the LYP correlation functional, J. Chem. Phys. 98 (1993) 5648-5652.

[19] C. Lee, W. Yang, R.G. Parr, Development of the Colle-Salvetti correlation-energy formula into a functional of the electron density, Phys. Rev. B37 (1988) 785-789.

[20] M. Tahenti, S. Gatfaoui, N. Issaoui, T. Roisnel, H. Marouani, A tetrachlorocobaltate(II) salt with 2-amino-5-picolinium: synthesis, theoretical and experimental characterization, J. Mol. Struct. 1207 (2020) 127781.

[21] C. Daghar, N. Issaoui, T. Roisnel, V. Dorcet, H. Marouani, J. Mol. Struct.1230 (2021) 129820.

[22] O. Noureddine, S. Gatfaoui, S. Antonia Brandán, A. Sagaama, H. Marouani, N. Issaoui, J. Mol. Struct. 1207 (2020) 127762.

[23] S.K. Wolff, D.J. Grimwood, J.J. McKinnon, D. Jayatilaka, M.A. Spackamn, CrystalExplorer 3.1, University of Westren Australia, Perth, 2013.

[24] T. Lu, F. Chen, Multiwfn: A multifunctional wavefunction analyzer, J. Comput. Chem. 33 (2012) 580-592.

[25] W. Humphrey, A. Dalke, K. Schulten, VMD: Visual molecular dynamics, J. Mol. Graph. 14 (1996) 33-38.

[26] S. Alvarez, M. Llunell, Continuous symmetry measures of penta-coordinate molecules: Berry and non-Berry distortions of the trigonal bipyramid, J. Chem. Soc. 19 (2000) 3288-3303.

[27] C. Jelsch, K. Ejsmont, L. Huder, The enrichment ratio of atomic contacts in crystals, an indicator derived from the Hirshfeld surface analysis, L. IUCrJ, 1 (2014) 119–128.

[28] S. Trabelsi, N. Issaoui, S. A. Brandán, F. Bardak, T. Roisnel, A. Atac, H. Marouani, J. Mol. Struct.1185 (2019) 168-182.

[29] S. Gatfaoui, N. Issaoui, T. Roisnel, H. Marouani, J. Mol. Struct. 191 (2019) 183-196.

[30] S. Gatfaoui, N. Issaoui, A. Mezni, F. Bardak, T. Roisnel, A. Atac, H. Marouani, J. Mol. Struct.1150 (2017) 242-257.

[31] S. Gatfaoui, N. Issaoui, T. Roisnel, H. Marouani, J. Mol. Struct. 1225 (2020) 129132.

[32] R.F.W. Bader, Atoms in Molecules, A Quantum Theory, Oxford University Press, Oxford, 1990, ISBN 0198558651.

[33] U. Koch, P. Popelier, Characterization of C-H-O hydrogen bonds on the basis ofthe charge density, J. Phys. Chem. Soc. A99 (1995) 9747.

[34] I. Rozas, I. Alkorta, J. Elguero, Behavior of ylides containing N, O, and C atoms as hydrogen bond acceptors, J. Am. Chem. Soc. 122 (2000) 11154-11161.

[35] P. Politzer, J. S. Murray, The fundamental nature and role of the electrostatic potential in atoms and molecules, Theor. Chem. Acc. 108 (2002) 134–142.

[36] N. Mohan, C. H. Suresh, A molecular electrostatic potential analysis of hydrogen, halogen and dihydrogen bonds, J. Phys. Chem. 118 (2014) 1697−1705.

Figure captions

Fig. 1. ORTEP representation of the asymmetric unit of $(C_6H_{14}N)_2[CdCl_4]$ with atom-labeling scheme. Displacement ellipsoids are drawn at the 50% probability level. H atoms are represented as small spheres of arbitrary radii. Hydrogen bonds are denoted as dashed lines **(a)** and the optimized molecular structure **(b)**.

Fig. 2. The packing of the title compound viewed along the *c*-axis **(a)**, while **(b,c,d,e)** represents a perspective view showing the disposition of the 1-D polymeric chains of the inorganic part and the patterns of hydrogen bonding in $(C_6H_{14}N)_2[CdCl_4]$, $CdCl_5$ is given in polyhedral representation. The dotted lines indicate the hydrogen bonds.

Fig. 3. 3D Hirshfeld surfaces mapped with d_{norm} in the range [-0.806 to 1.173] of $(C_6H_{14}N)_2[CdCl_4]$, red dotted lines represent hydrogen bonds. (iii) x, −y, z−1/2.

Fig. 4. 2D fingerprint plots of the full **(a)** and the main intercontacts showing percentage of various intermolecular contacts contributed to the Hirshfeld surface $(C_6H_{14}N)_2[CdCl_4]$ **(b,c,d,e,f).** Surface to the side **(g)** highlight the relevant surface patch associated with H…Cl/Cl…H contacts.

Fig. 5. Theoretical and experimental IR spectrum of $(C_6H_{14}N)_2CdCl_4$.

Fig. 6. AIM molecular graph screening the different bond critical points (BCPs) of $(C_6H_{14}N)_2CdCl_4$. The BCPs are represented by small orange balls and the connecting paths by orange lines.

Fig. 7. Plots of the reduced density gradient scatter **(a)**, and color-filled isosurface of the $(C_6H_{14}N)_2[CdCl_4]$ complex illustrating the non-bonded interactions **(b)**.

Fig. 8. Molecular electrostatic potential surface (MEPs) of $(C_6H_{14}N)_2[CdCl_4]$.

Fig. 9. The frontier molecular orbitals of $(C_6H_{14}N)_2CdCl_4$ molecule at DFT/LANL2DZ level.

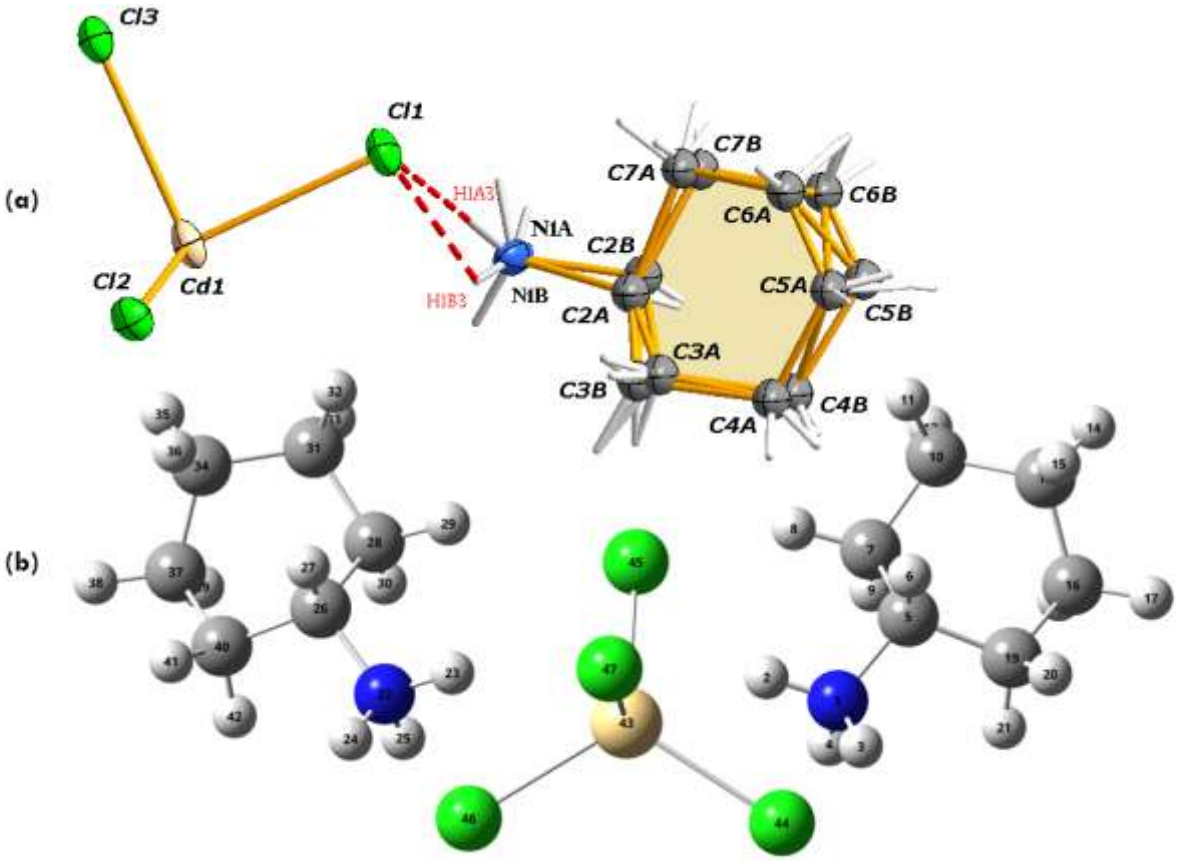

Fig. 1. ORTEP representation of the asymmetric unit of $(C_6H_{14}N)_2[CdCl_4]$ with atom-labeling scheme. Displacement ellipsoids are drawn at the 50% probability level. H atoms are represented as small spheres of arbitrary radii. Hydrogen bonds are denoted as dashed lines **(a)** and the optimized molecular structure **(b)**.

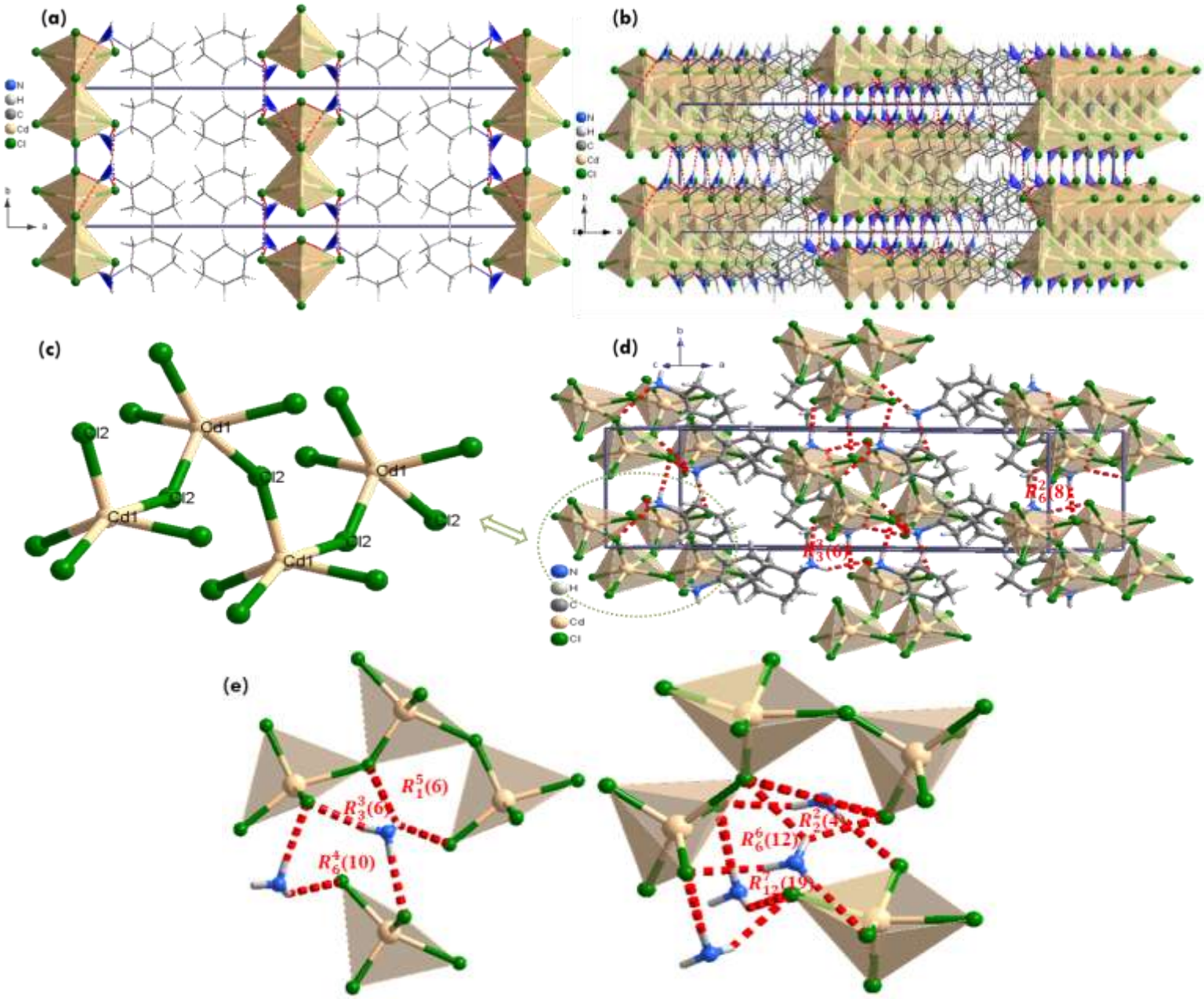

Fig. 2. The packing of the title compound viewed along the *c*-axis **(a)**, while **(b,c,d,e)** represents a perspective view showing the disposition of the 1-D polymeric chains of the inorganic part and the patterns of hydrogen bonding in $(C_6H_{14}N)_2[CdCl_4]$, $CdCl_5$ is given in polyhedral representation. The dotted lines indicate the hydrogen bonds.

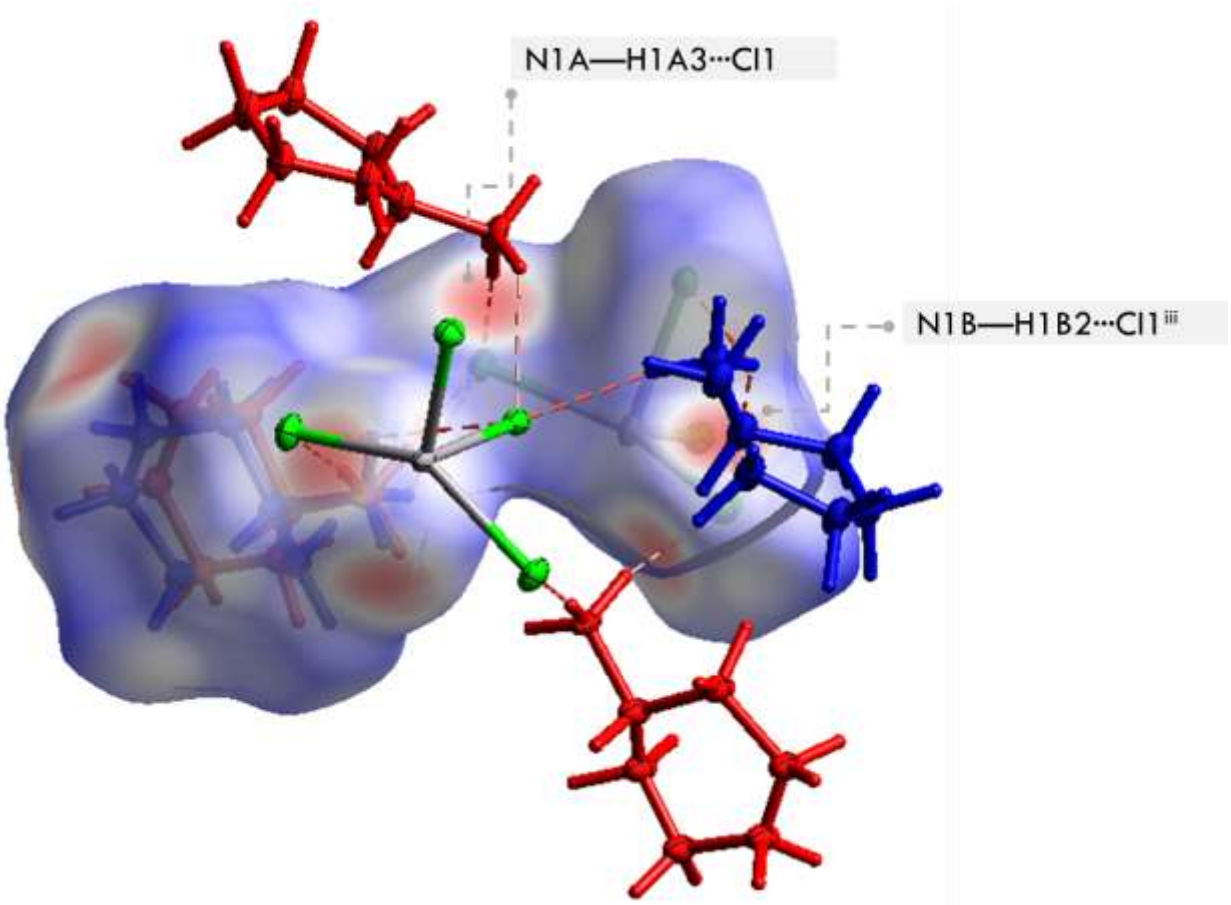

Fig. 3. 3D Hirshfeld surfaces mapped with d_{norm} in the range [-0.806 to 1.173] of $(C_6H_{14}N)_2[CdCl_4]$, red dotted lines represent hydrogen bonds. (iii) x, −y, z−1/2.

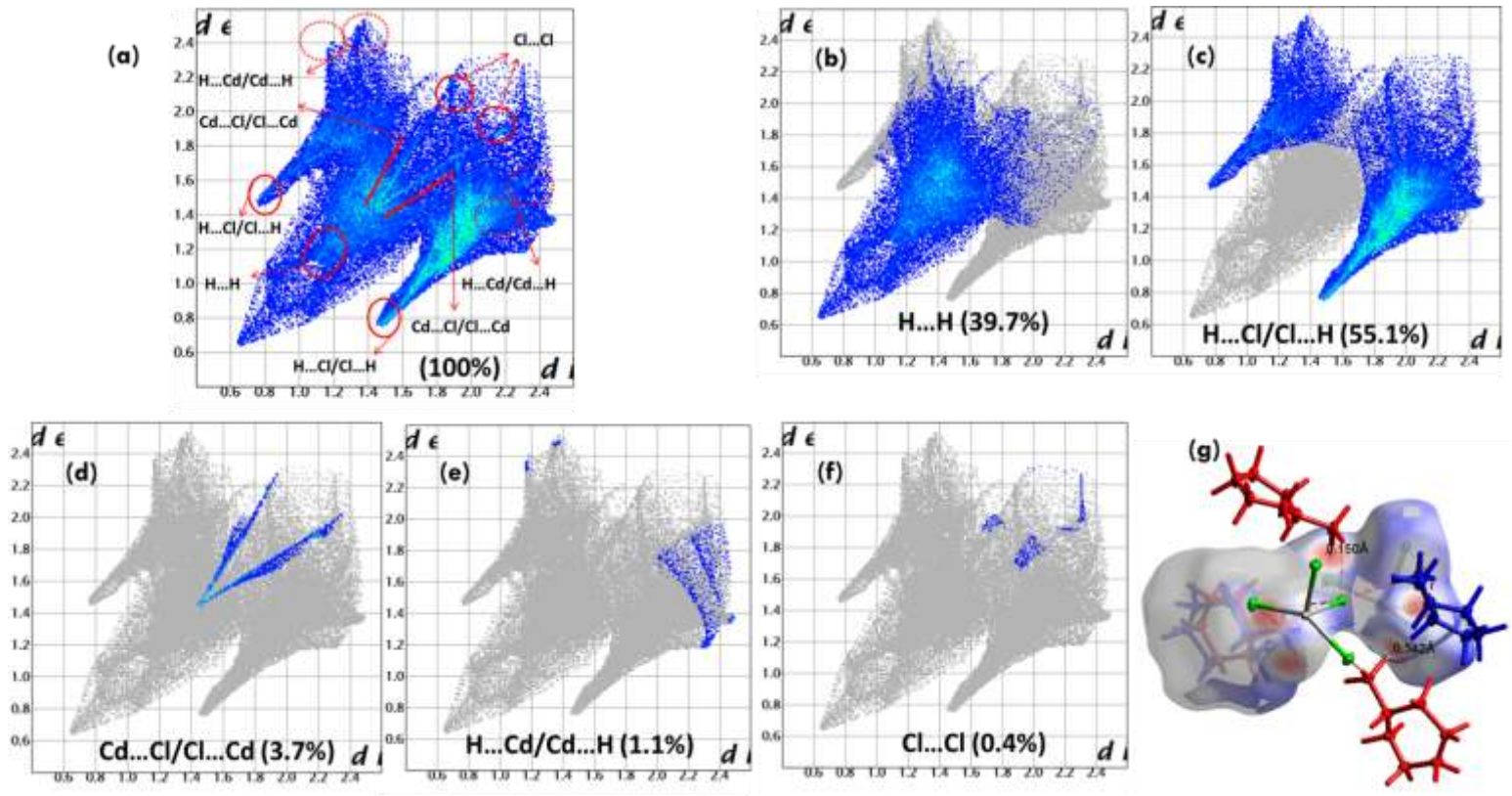

Fig. 4. 2D fingerprint plots of the full **(a)** and the main intercontacts showing percentage of various intermolecular contacts contributed to the Hirshfeld surface $(C_6H_{14}N)_2[CdCl_4]$ **(b,c,d,e,f).** Surface to the side **(g)** highlight the relevant surface patch associated with H…Cl/Cl…H contacts.

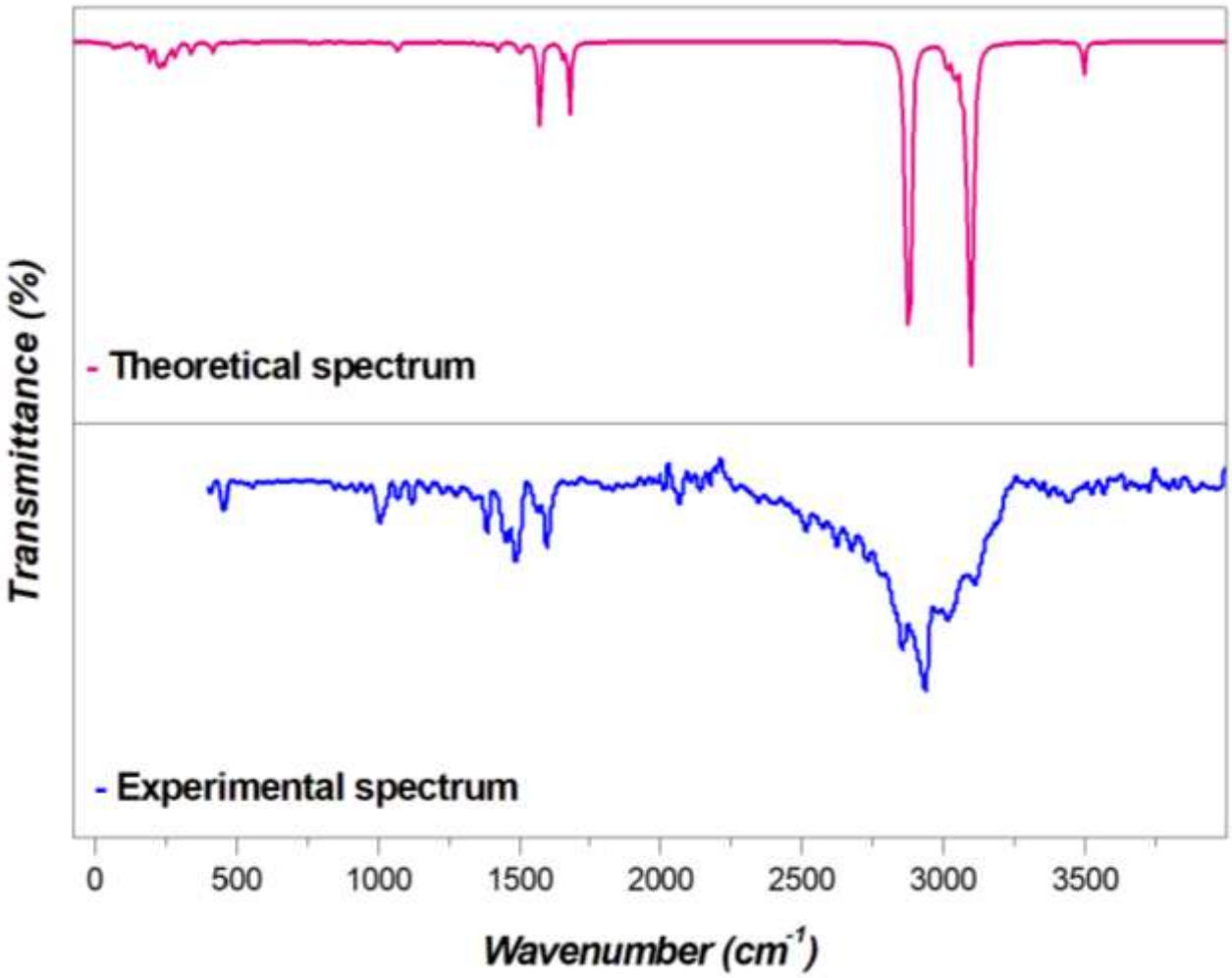

Fig. 5. Theoretical and experimental IR spectrum of $(C_6H_{14}N)_2CdCl_4$.

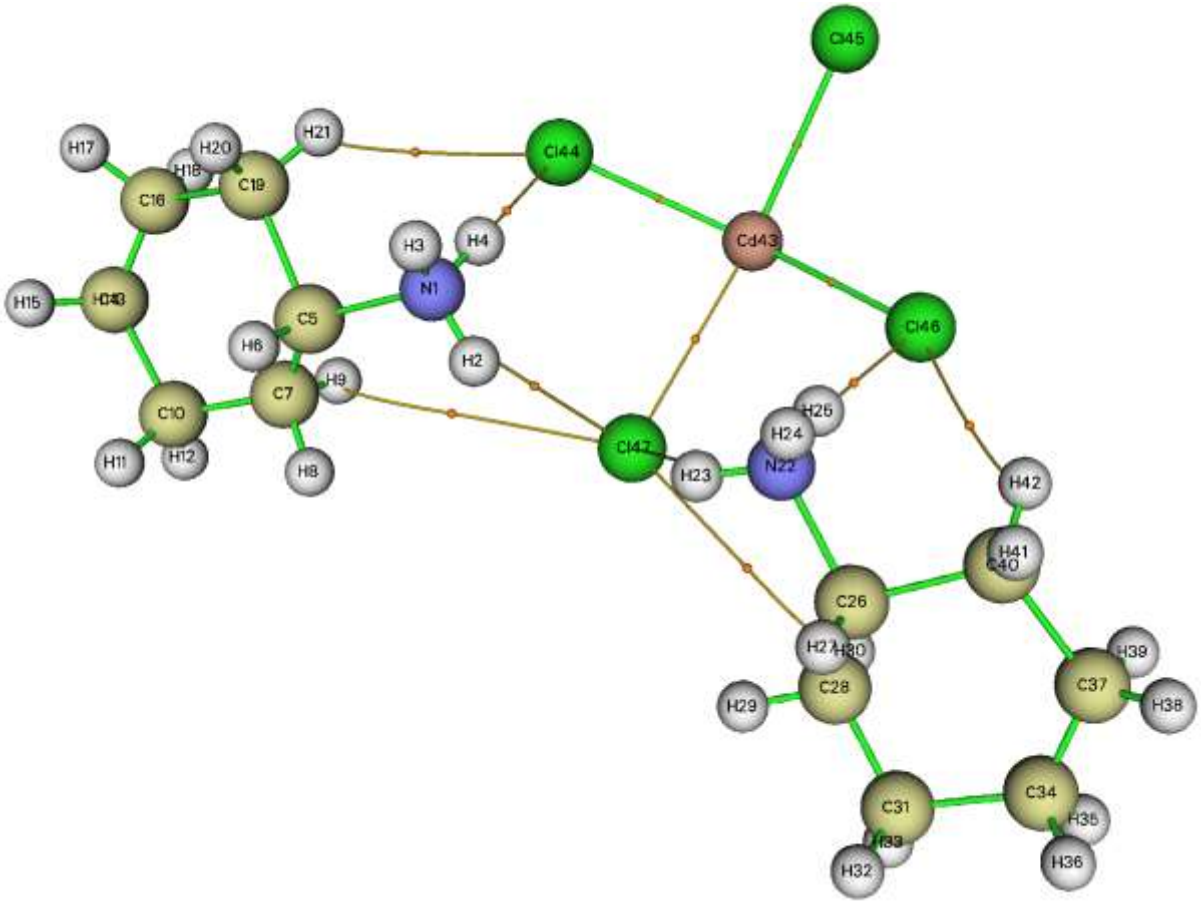

Fig. 6. AIM molecular graph screening the different bond critical points (BCPs) of $(C_6H_{14}N)_2CdCl_4$. The BCPs are represented by small orange balls and the connecting paths by orange lines.

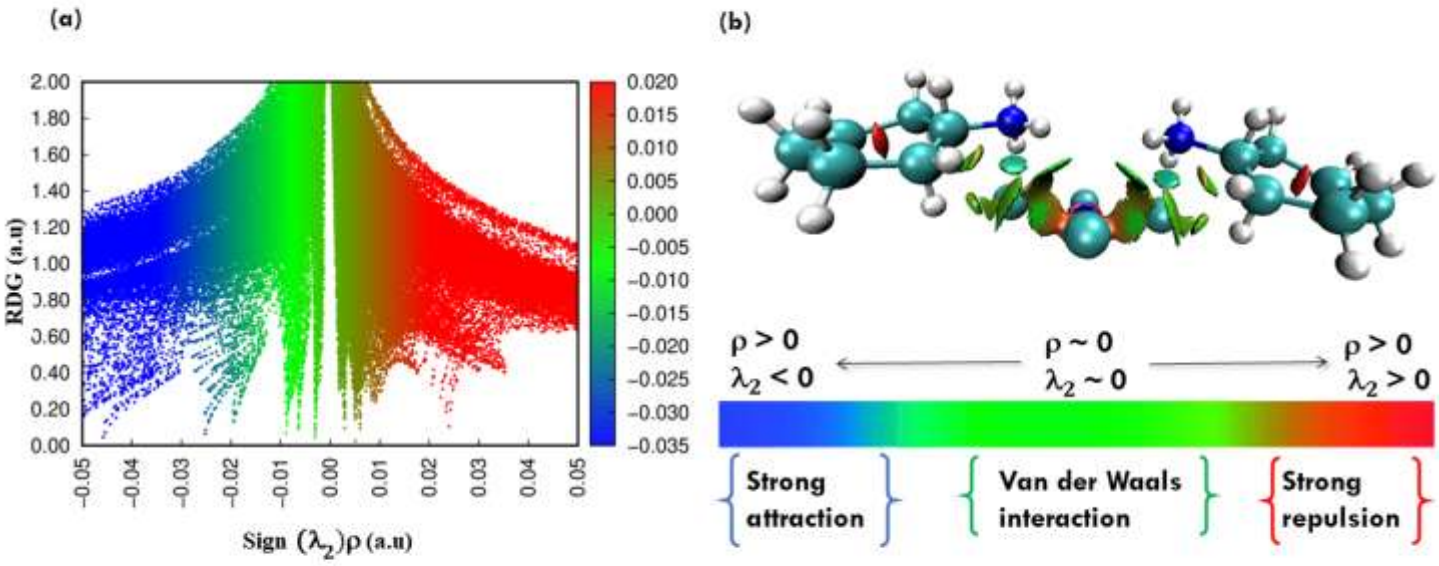

Fig. 7. Plots of the reduced density gradient scatter **(a)**, and color-filled isosurface of the $(C_6H_{14}N)_2[CdCl_4]$ complex illustrating the non-bonded interactions **(b)**.

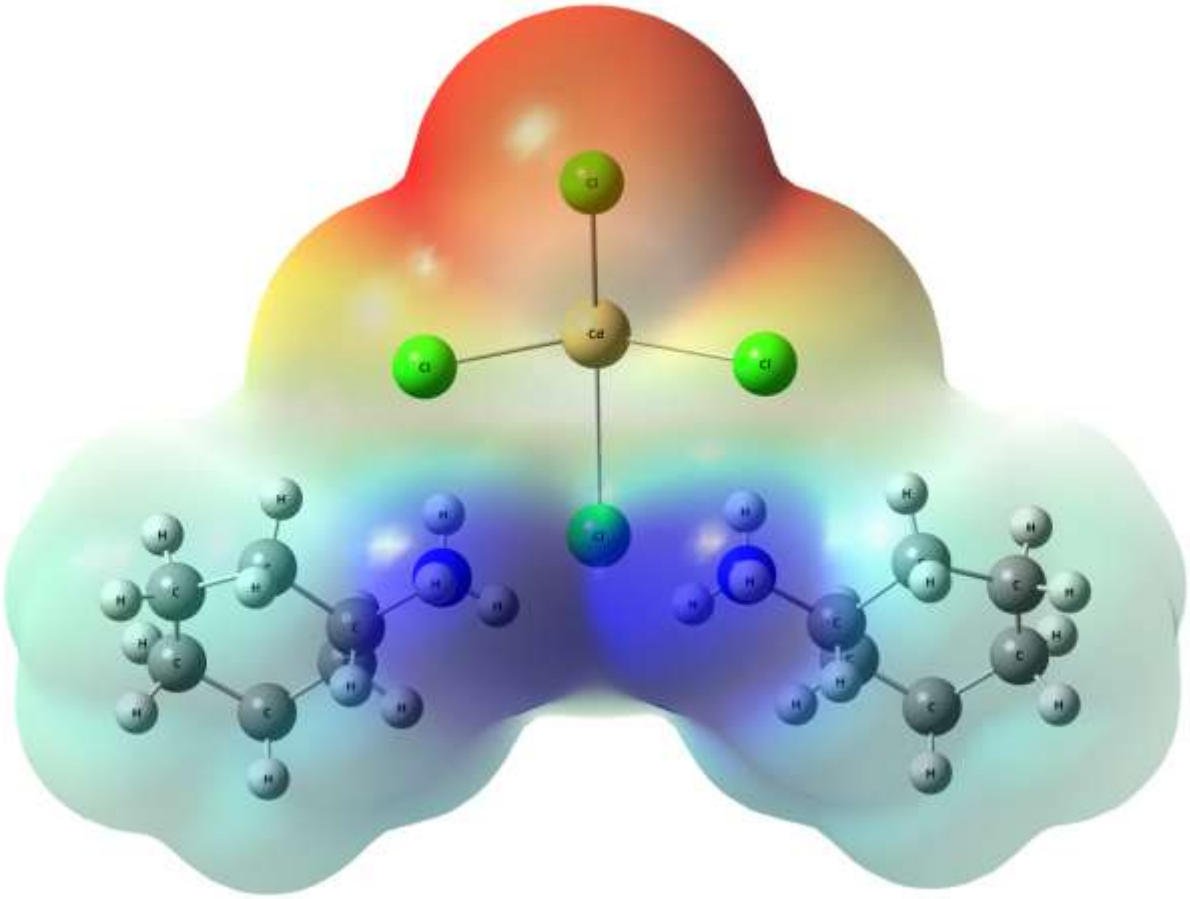

Fig. 8. Molecular electrostatic potential surface (MEPs) of $(C_6H_{14}N)_2[CdCl_4]$.

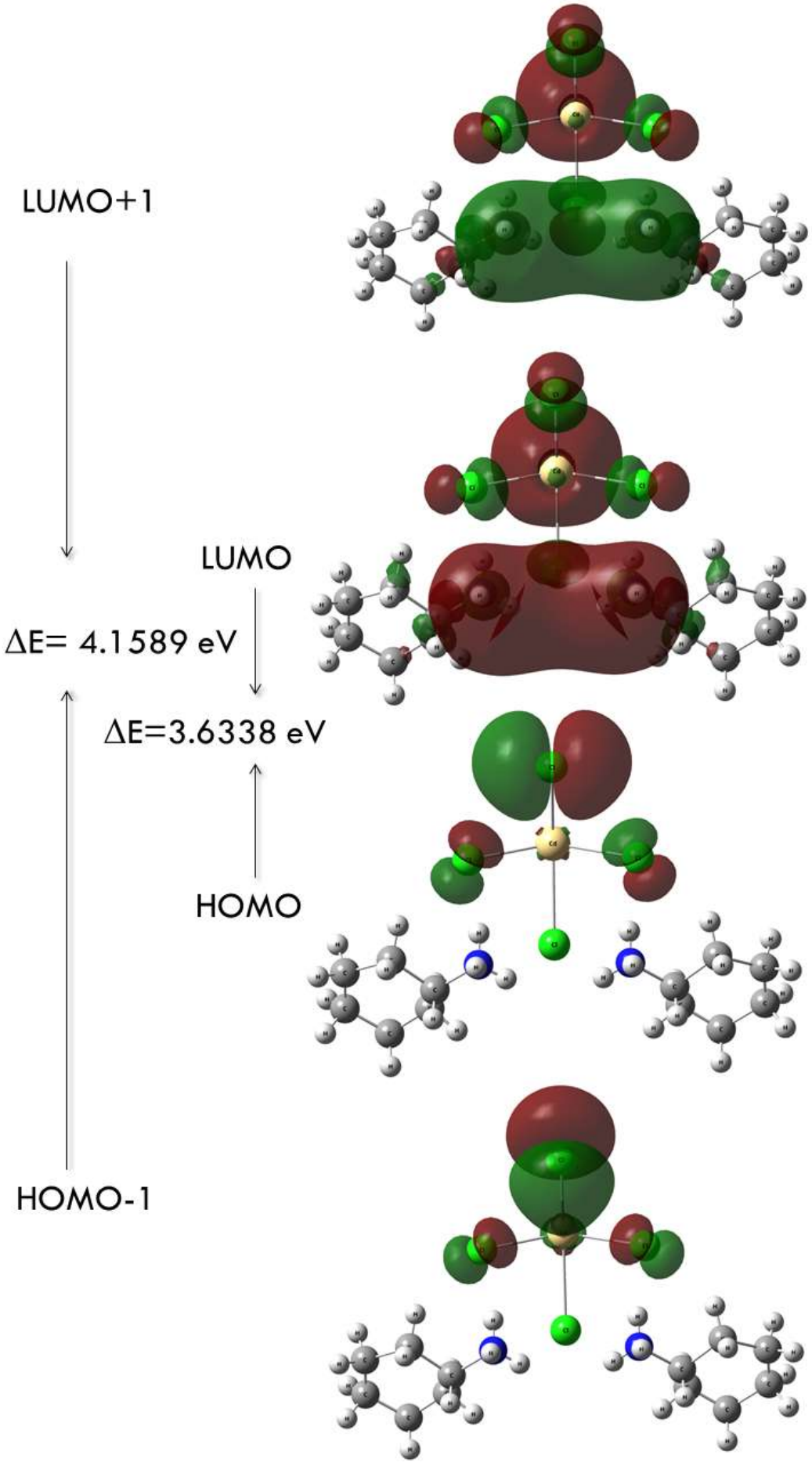

Fig. 9. The frontier molecular orbitals of $(C_6H_{14}N)_2CdCl_4$ molecule at DFT/LANL2DZ level.

Table captions

Table 1. Crystal data and structure refinement parameters for $(C_6H_{14}N)_2CdCl_4$.

Table 2. Principal intermolecular distances (Å) and bond angles (°) in $(C_6H_{14}N)_2CdCl_4$ by X-ray data (with estimated standard deviation in parentheses) and by theoretical calculations.

Table 3. Hydrogen-bonds geometry (Å, °) of $(C_6H_{14}N)_2CdCl_4$.

Table 4. Global reactivity descriptors and calculated energy values of $(C_6H_{14}N)_2CdCl_4$ at DFT/LANL2DZ level.

Table 5. The electric dipole moment, polarizability, and first order hyperpolarizability values of $(C_6H_{14}N)_2CdCl_4$.

Table 1. Crystal data and structure refinement parameters for $(C_6H_{14}N)_2CdCl_4$.

CCDC	2068977
Temperature	150 K
Empirical formula	$2(C_6H_{14}N)CdCl_4$
Formula weight (g mol^{-1})	454.56
Crystal system	Orthorhombic
Space group	$Cmc2_1$
a	27.257 (2)Å
b	8.3560 (6) Å
c	7.8872 (5)Å
Z	4
V	1796.4 (2)$Å^3$
F(000)	920
μ(Mo Kα)	1.80 mm^{-1}
Index ranges	$-35 \leq h \leq 26$, $-10 \leq k \leq 10$, $-9 \leq l \leq 10$
Reflections collected	7344
Independent reflections	2013
Reflections with $I > 2\sigma(I)$	1985
R_{int}	0.034
$(\sin\theta/\lambda)_{max}$ ($Å^{-1}$)	0.649
Absorption correction: multi-scan	T_{min}= 0.574, T_{max} = 0.723
Refined parameters	82
$R[F^2> 2\sigma(F^2)]$	0.044
$wR(F^2)$	0.114
Goodness of fit	1.11
Absolute structure parameter	-0.04 (9)
$\Delta\rho_{max}$ = 1.93e $Å^{-3}$	$\Delta\rho_{min}$ = −0.90e $Å^{-3}$

Table 2. Principal intermolecular distances (Å) and bond angles (°) in $(C_6H_{14}N)_2CdCl_4$ by X-ray data (with estimated standard deviation in parentheses) and by theoretical calculations.

Bond length (Å)			**Bond angles (°)**		
	Calculated B3LYP 6-311++G(d.p)	X-Ray		Calculated B3LYP 6-311++G(d.p)	X-Ray
Inorganic					
Cd1—Cl1	2.516	2.5105 (19)	Cl1—Cd1—Cl2	117.7369	108.15 (5)
Cd1—Cl3	2.435	2.604 (3)	Cl1i—Cd1—Cl2	117.7371	108.15 (5)
Cd1—Cl1^{i}	2.516	2.5105 (19)	Cl1—Cd1—Cl1^{i}	116.0749	142.89 (11)
Cd1—Cl2	2.760	2.489 (3)	Cl2—Cd1—Cl3	100.8358	103.69 (10)
Cd1—Cl2^{ii}	2.898	2.892 (3)	Cl1—Cd1—Cl3	99.2208	89.37 (6)
			Cl1^{i}—Cd1—Cl3	99.22	89.37 (6)
			Cl1^{i}—Cd1—Cl2^{ii}	85.835	83.30 (6)
			Cl3—Cd1—Cl2^{ii}	153.22	156.53 (9)
Organic					
C2A—C3A	1.528	1.18 (3)	N1A—C2A—C7A	105.4	101.3 (13)
C2A—C7A	1.543	1.60 (3)	C3A—C2A—C7A	110.3	118.9 (19)
C3A—C4A	1.546	1.40 (3)	C2A—C3A—C4A	109.0	126 (3)
C4A—C5A	1.549	1.51 (3)	C3A—C4A—C5A	108.1	110.1 (18)
C5A—C6A	1.533	1.26 (2)	C6A—C5A—C4A	110.1	123.8 (16)
C6A—C7A	1.546	1.60 (3)	C5A—C6A—C7A	109.1	120.1 (17)
N1A—C2A	1.507	1.564 (19)	C6A—C7A—C2A	109.4	107.2 (16)
N1B—C2B	1.507	1.53 (2)	N1B—C2B—C3B	105.4	97.4 (14)
C2B—C7B	1.528	1.51 (3)	C7B—C2B—C3B	110.3	113.4 (17)
			C5B—C4B—C3B	108.1	116.2 (16)

Symmetry codes: (i) −*x*+1, *y*, *z*; (ii) *x*, −*y*+1, *z*−1/2.

Table 3. Hydrogen-bonds geometry (Å, °) of $(C_6H_{14}N)_2CdCl_4$.

D—H···A	D—H (Å)	H···A (Å)	D···A (Å)	D—H···A (°)
N1A—H1A1···Cl3^{i}	0.91	2.51	3.199 (5)	133
N1A—H1A1···Cl2^{ii}	0.91	2.82	3.372 (6)	121
N1A—H1A2···Cl1^{iii}	0.91	2.34	3.248 (6)	176
N1A—H1A3···Cl1	0.91	2.34	3.223 (5)	165
N1B—H1B1···Cl3^{i}	0.91	2.31	3.199 (5)	164
N1B—H1B2···Cl1^{iii}	0.91	2.75	3.248 (6)	116
N1B—H1B2···Cl3^{iii}	0.91	2.79	3.289 (5)	116
N1B—H1B3···Cl1	0.91	2.58	3.223 (5)	128
N1B—H1B3···Cl2^{ii}	0.91	2.65	3.372 (6)	137

Symmetry codes: (i) x, y, z−1; (ii) x, −y+1, z−1/2; (iii) x, −y, z−1/2.

Table 4. Global reactivity descriptors and calculated frontier molecular orbital parameters of $(C_6H_{14}N)_2CdCl_4$ using DFT/LANL2DZ level.

Energies (eV)		Ionization potential A	1.51594704
Frontier orbitals		Electron affinity I	5.14975726
E_{HOMO}	-5.14975726	Descriptors	
E_{LUMO}	-1.51594704	Global electrophilicity (ω)	3.05681992
$\lvert E_{HOMO}-E_{LUMO}\rvert$	3.63381022	Electronegativity (χ)	3.33285215
E_{HOMO-1}	-5.32663135	Global chemical potential (μ)	-3.33285215
E_{LUMO+1}	-1.16764113	Global hardness (η)	1.81690511
$\lvert E_{HOMO-1}-E_{LUMO+1}\rvert$	4.15899022	Global softness (S)	0.27519324

Table 5. The electric dipole moment, polarizability, and first order hyperpolarizability values of $(C_6H_{14}N)_2CdCl_4$.

Parameters	Value	Parameters	Value
α_{xx}	286.790	β_{xxx}	-0.0107938
α_{xy}	0.001	β_{xxy}	185.4371305
α_{xz}	228.937	β_{xyy}	-0.0007873
α_{yy}	0.001	β_{yyy}	-30.0793514
α_{yz}	-7.337	β_{xxz}	166.0728961
α_{zz}	207.967	β_{xyz}	0. 0098508
α_{total} (esu)	**241.23115 a.u.**	β_{yyz}	73.2899313
μ_x	-0.0006	β_{xzz}	0.0057606
μ_y	5.3605	β_{yzz}	-43.3495628
μ_z	8.6194	β_{zzz}	61.8600993
μ_{total} (D)	**10.1503**	**β (esu)**	**321.37376 a.u.**